Adiabaticity in the lateral electron-momentum distribution after strong-field ionization

Jost Henkel,[1,2] Manfred Lein,[1] Volker Engel,[2] and Ingo Dreissigacker[1]

[1]*Institut für Theoretische Physik and Centre for Quantum Engineering and Space-Time Research, Leibniz Universität Hannover,*
Appelstraße 2, D-30167 Hannover, Germany

[2]*Institut für Physikalische and Theoretische Chemie, Universität Würzburg, and Röntgen Research Center for Complex Material Systems,*
Emil-Fischer-Straße 42, D-97074 Würzburg, Germany

By solving the time-dependent Schrödinger equation for atoms in short laser pulses of different polarizations, it is shown that in strong-field ionization without rescattering, the lateral width of the electron-momentum distribution corresponds adiabatically to the instantaneous laser field on a sub-laser-cycle time scale, as expected in pure tunneling ionization. In contrast to the distributions along the polarization direction, the width is affected little by depletion or Coulomb effects.

Over the past three decades, rapid progress has been made in the development of lasers capable of producing strong pulses in the femtosecond regime. This had led to progress in many areas ranging from above-threshold ionization (ATI) [1] over high-order harmonic generation [2] and attosecond pulse generation [3] to laser-induced fragmentation of molecules [4,5], to name just a few. Many of the phenomena induced by strong fields have been explained on the basis of tunneling ionization. Tunneling is a purely quantum mechanical process, which is considered as one of the main differences from classical mechanics. Frequently, a semiclassical two-step model is invoked, which assumes that ionization leads to the birth of an unbound electron at the outer exit of the laser-induced tunneling barrier. After appearing in the classically allowed region, the electron motion is modeled by a Newtonian trajectory [6]. This has been used for many purposes, e.g., to derive cutoff laws in ATI [7,8], to describe Coulomb focusing [9], to correct the strong-field approximation for elliptically polarized fields [10], and to model the momentum distribution in angular streaking [11]. The semiclassical model is also the basis for the three-step model of high-order harmonic generation [12].

For an understanding of strong-field processes it is essential to verify the validity of the tunneling and semiclassical pictures. Along these lines, attosecond angular streaking [13–15], originally proposed to measure the carrier-envelope phase of few-cycle pulses [16], has been utilized to put a small upper limit on the tunneling delay time between the maximum of the electric field and the appearance of the escaping electron [17], thus giving insight into strong-field ionization on extremely short time scales. The interpretation of the momentum spectra in angular streaking, however, is complicated by Coulomb effects on the electron trajectories after tunneling and furthermore it is restricted to the intensity range below saturation [11]. It is desirable to overcome these limitations of angular streaking.

Recently, the importance of the lateral momentum distribution, i.e., the distribution in the direction perpendicular to the laser field, has been recognized [18–20]. If not modified by electron recollision, the lateral distribution carries direct information about the ionization step since there is no laser-induced force in this direction. The tunneling ionization rate

decreases with increasing lateral momentum approximately as a Gaussian. The width of the Gaussian is proportional to the square root of the electric field [21]. Multiplying this tunneling filter with the ground-state momentum distribution thus leads to a simple product formula for the lateral distribution [22]. This has been exploited to improve [23] the measurement of laser peak intensities via momentum distributions [24]. The measured widths from circularly polarized fields [20] are about 15% above the values predicted by the product formula, suggesting that nonadiabatic corrections [25] might cause such a deviation. However, the measurement did not show a significant wavelength dependence.

For the hydrogen atom we show, by solving the time-dependent Schrödinger equation (TDSE), that the lateral widths of the momentum distributions produced by infrared fields are in excellent agreement with the exact adiabatic widths from static calculations, without the need to invoke nonadiabatic effects. We confirm that the width follows the instantaneous electric field on the sub-laser-cycle time scale. Moreover, we demonstrate that the width is, in contrast to the momentum distribution in the field direction, only negligibly affected by depletion and it is less sensitive to Coulomb corrections. It can therefore serve as a more reliable observable in angular streaking. Results for higher laser frequencies suggest that nonadiabatic effects tend to narrow the lateral distribution, in contrast to the widening predicted by the nonadiabatic corrections to the tunneling formula [20,25].

We perform TDSE simulations in cylindrical coordinates for the H atom in linearly polarized (LP) half-cycle pulses as well as full three-dimensional (3D) calculations for circularly polarized (CP) few-cycle pulses. These special cases have been selected to avoid contamination by recollisions. The laser frequency ω is 0.0569 a.u., corresponding to a wavelength of 800 nm, except when specified differently. The TDSE reads (atomic units are used throughout, i.e., $\hbar = e = m_e = 1$)

$$i\,\partial_t \psi = [-\nabla^2/2 + v(r) + W(t)]\psi, \tag{1}$$

where $W(t)$ is the laser-atom interaction in the dipole approximation and $v(r)$ is the atomic potential. The wave function is propagated using the split-operator method [26]. In the case of the LP half-cycle pulse, we use the length gauge $W(t) = \mathbf{r} \cdot \mathbf{E}(t) = z E_0 \sin(\omega t)$, with the electric-field

amplitude E_0 and the potential $v(r) = -1/r$ of the H atom. Here we solve the TDSE in cylindrical coordinates with a time step of 0.0125 a.u. on a grid with 1536 points in the radial direction and 6144 points in the field direction, covering lengths of 225 and 900 a.u., respectively. The propagation is continued after the pulse until the electron wave packet is sufficiently far from the nucleus to neglect the Coulomb field. We then obtain the final momentum distribution $|\tilde{\psi}(\mathbf{k})|^2$ from the outgoing wave packet. In the case of the three-cycle CP laser pulse, we use the velocity gauge $W(t) = \mathbf{p} \cdot \mathbf{A}(t)$, with the vector potential

$$\mathbf{A}(t) = A_0 \sin^2(\omega t/6)[\mathbf{e}_x \sin(\omega t) - \mathbf{e}_y \cos(\omega t)] \quad (2)$$

for $t \in [0; 6\pi/\omega]$. The electric field $\mathbf{E}(t) = -\dot{\mathbf{A}}(t)$ has the maximum strength $E_0 = A_0\omega$. To keep the 3D CP simulations manageable for high intensities, we employ a soft-core potential $v(r) = -1/\sqrt{r^2 + 0.2}$, which yields the ground-state energy -0.364 a.u. The grid comprises 512 points for a length of 400 a.u. in each Cartesian coordinate and the time step is 0.32 a.u. The final momentum distribution $|\tilde{\psi}(\mathbf{k})|^2$ of the outgoing electrons is obtained as in Ref. [27].

For analysis of the LP results, we calculate the longitudinal momentum distribution

$$P^{\mathrm{LP}}(k_z) = \iint dk_x dk_y |\tilde{\psi}(k_x, k_y, k_z)|^2 \quad (3)$$

and lateral distributions

$$Q^{\mathrm{LP}}_{k_z}(k_\perp) = \int dk_x |\tilde{\psi}(k_x, k_\perp, k_z)|^2 \quad (4)$$

at every k_z. Here and in the following, $k_\perp$ always denotes a momentum component perpendicular to the electric field. Analogously, in the case of the CP calculation, we compute the angular distribution over the azimuth φ,

$$P^{\mathrm{CP}}(\varphi) = \iint dk_\perp dk_\parallel k_\parallel |\tilde{\psi}(k_\parallel \cos\varphi, k_\parallel \sin\varphi, k_\perp)|^2, \quad (5)$$

and lateral distributions

$$Q^{\mathrm{CP}}_\varphi(k_\perp) = \int_{k_i}^\infty dk_\parallel k_\parallel |\tilde{\psi}(k_\parallel \cos\varphi, k_\parallel \sin\varphi, k_\perp)|^2 \quad (6)$$

at every angle φ. The integration normally starts at $k_i = 0$, but k_i is set to larger values for high laser intensities, as explained later.

In a semiclassical two-step model accounting for depletion, the momentum distributions are written as [28]

$$P^{\mathrm{LP\,or\,CP}}(q) = dN/dq = N_b(t_0)\,\Gamma(E(t_0))\,dt_0/dq, \quad (7)$$

with $q = k_z$ for the LP half-cycle pulse and $q = \varphi$ for the CP pulse. In Eq. (7), dN is the number of escaping electrons in the range from q to $q + dq$. The number of bound electrons $N_b(t_0)$ is taken from the solution of the TDSE. It accounts for depletion effects. The ionization rate $\Gamma(E)$ in a static electric field E provides the instantaneous ionization rate at the time of ionization t_0. The values for Γ are taken from the literature [29–31] in the case of the half-cycle pulse. For the CP pulse,
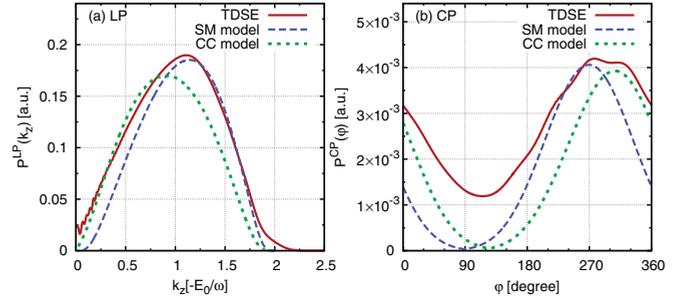

FIG. 1. (Color online) (a) Longitudinal momentum distribution $P^{\mathrm{LP}}(k_z)$ at $E_0 = 0.12$ a.u. and (b) angular distribution $P^{\mathrm{CP}}(\varphi)$ at $E_0 = 0.027$ a.u. from the TDSE and the two semiclassical SM and CC models.

Γ is approximated using the tunneling formula [32]

$$\Gamma(E) = \Gamma_0 \exp[-2(2I_p)^{3/2}/3E], \quad (8)$$

with the ionization potential I_p. The pre-exponential factor Γ_0 is adjusted to match the TDSE results. The relation between the initial time t_0 and the final momentum k_z (final angle φ) is evaluated using classical trajectories within two different models: (i) the simple man's (SM) model, in which the force on the electron includes only the laser field, and (ii) the Coulomb corrected (CC) model, accounting also for the interaction with the nucleus. In both models, the initial velocity of the electron is zero [33], except when the laser intensity is in the over-the-barrier ionization region [34] in the CC model. In this case, the initial velocity is set equal to $\sqrt{2\{\mathcal{E}_0 - [v(r_0) + \mathbf{E}(t_0) \cdot \mathbf{r}_0]\}}$, with the ground-state energy $\mathcal{E}_0$ and the starting point $\mathbf{r}_0$ of the electron trajectory. In the over-the-barrier ionization region, $\mathbf{r}_0$ is chosen to be the saddle point of the barrier function $v(r) + \mathbf{E}(t) \cdot \mathbf{r}$, while for lower intensities it is set equal to the tunneling exit. In the LP calculations, the ground-state energy $\mathcal{E}_0$ has been modified to account for the Stark shift and we use the decoupled equations in parabolic coordinates for calculating the starting point [35] as well as the subsequent classical trajectories.

Typical results for the longitudinal and angular distributions from moderate fields are shown in Fig. 1. They confirm our expectation of finding the strongest ionization near the time of maximum electric field, i.e., midpulse, leading to maximum emission near $k_z = -E_0/\omega$ in the LP case and near the angle $\varphi = 270°$ in the CP case. Both SM and CC models are in reasonable agreement with the TDSE results. Momentum distributions from the CP calculation, integrated along k_z, are shown in Fig. 2 for two different intensites. For the lower intensity, we find the maximum emission at approximately $\varphi = 270°$, whereas for the higher intensitiy, we observe strong depletion, shifting the maximum emission toward earlier times, corresponding to angles of approximately 90° [see Fig. 2(b)].

The purpose of this Rapid Communication is a precise investigation of the lateral width and a comparison with tunneling and exact adiabatic calculations. According to the simplified tunneling model, the lateral distribution has the product form [20,22]

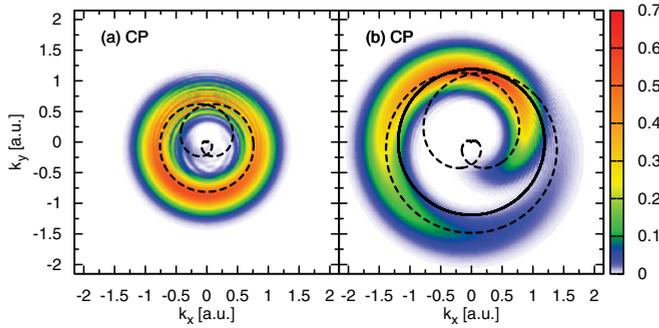$$Q(k_\perp) = Q_0(k_\perp) \exp(-k_\perp^2 \tau), \quad (9)$$

FIG. 2. (Color online) Momentum distribution from three-cycle CP pulses, integrated along k_z into the xy plane of polarization at (a) $E_0 = 0.046$ a.u. and (b) $E_0 = 0.084$ a.u. The dotted curves show the predictions of the SM model, while the solid black curve in (b) indicates the lower integration limit k_i for Eq. (6).

where $\tau = \sqrt{2I_p}/E(t_0)$ is the tunneling time for ionization at t_0. The weakly field-dependent $Q_0(k_\perp)$ is obtained from the ground-state momentum distribution $\tilde{\psi}_0(k_x, k_y, k_z)$ as

$$Q_0(k_\perp) = \iint dk_\parallel dk'_\perp |\tilde{\psi}_0(k_\parallel, k'_\perp, k_\perp)|^2 \exp(-k'^2_\perp \tau). \quad (10)$$

For the LP pulse, we additionally calculate the exact adiabatic lateral distribution, where we exploit the fact that the static Schrödinger equation (SSE) for the H atom in a static field,

$$(-\nabla^2/2 - 1/r + Ez)\psi_0 = \mathcal{E}\psi_0, \quad (11)$$

is separable via $\psi_0 = M(\mu)N(\nu)\exp(im\varphi)$ in squared parabolic coordinates μ, ν, φ [30], such that $x = \mu\nu\cos\varphi$, $y = \mu\nu\sin\varphi$, and $z = 1/2(\mu^2 - \nu^2)$. We solve the SSE with outgoing boundary conditions [30]. The complex energies $\mathcal{E} = \mathcal{E}_0 - i\Gamma/2$, with the Stark-shifted ground-state energy $\mathcal{E}_0$ and the ionization rate Γ, are taken from Refs. [29–31].

The resulting lateral distributions $Q^{LP}_{k_z}(k_\perp)$ and $Q^{CP}_\varphi(k_\perp)$, both from the TDSE and the models, are fitted to Gaussians $\exp(-k^2_\perp/\sigma^2)$ to obtain the lateral widths $\sigma^{LP}(k_z)$ and $\sigma^{CP}(\varphi)$, respectively. In the case of very strong fields (distinct depletion effects), contributions from more than one optical cycle contribute to emission at the same angle, but with different energies, as can be seen in Fig. 2(b). Here the lower integration limit k_i in Eq. (6) has been chosen such that between $180°$ and $360°$ only the contribution from the central half cycle enters into $Q^{CP}_\varphi(k_\perp)$, as indicated by the black solid circle in Fig. 2(b).

The calculated widths are shown in Fig. 3. For this figure the SM model is used to link the final momentum (final angle) to the instantaneous field needed by the adiabatic and tunneling models. In agreement with the SM model, the TDSE widths $\sigma^{LP}(k_z)$ and $\sigma^{CP}(\varphi)$ maximize at $k_z = -E_0/\omega$ and $\varphi = 270°$, respectively. Furthermore, it is striking how the width follows the instantaneous field strength on a sub-laser-cycle time scale. In fact, for the LP pulse there is excellent agreement between the TDSE width and the adiabatic width from the SSE, even in the case of the dramatic depletion shown in Fig. 3(a), where the maximum signal is shifted to a longitudinal momentum far from $k_z = -E_0/\omega$. We have also numerically confirmed for the soft-core potential that the maximum widths from a
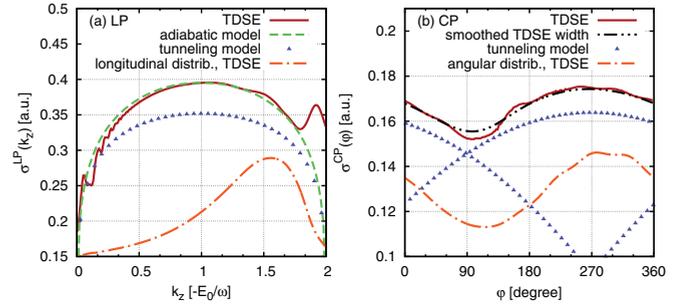

FIG. 3. (Color online) (a) Width $\sigma^{LP}(k_z)$ obtained at $E_0 = 0.2$ a.u. from the TDSE, the exact adiabatic model, and the tunneling model. (b) Width $\sigma^{CP}(\varphi)$ obtained at $E_0 = 0.027$ a.u. from the TDSE and the tunneling model. Also shown are the corresponding TDSE longitudinal and angular distributions $P^{LP}(k_z)$ and $P^{CP}(\varphi)$, respectively (not to scale). Tunneling model refers to the tunneling product formula [Eq. (9)] combined with the SM model.

half-cycle LP pulse and from the three-cycle CP pulse differ negligibly (not shown).

Our results suggest a streaking technique that links the maximum of the instantaneous field to the maximum measured width instead of the maximum measured signal as in [13]. To this end we find the locations and values of the maxima over a broad range of laser intensities. In view of the wiggles found in the low-intensity angular dependence of the TDSE width $\sigma^{CP}(\varphi)$ [see Fig. 3(b)], we find the maximum after convoluting with a Gaussian $\exp[-0.5(\varphi/\delta)^2]$ with $\delta = 30°$ for low fields up to $E_0 = 0.05$ a.u. and $\delta = 15°$ for stronger fields. The same procedure was applied to the angular distributions.

The positions of the maxima are shown in Figs. 4 and 5. In the case of the LP half-cycle pulse, we observe in the TDSE calculation a shift of the maximum of the longitudinal distribution to momenta with absolute values below E_0/ω for small fields and a shift to higher values for strong fields [Fig. 4(a)]. Only in the intermediate region around $E_0 \approx 0.1$ a.u. is the maximum really located at $-E_0/\omega$. Analogously, we find that the maximum of the angular distribution in the case of the CP pulse is shifted toward greater angles for low fields and to smaller angles φ for strong fields [Fig. 5(a)]. The shift at high fields can mostly be explained by the depletion effect [16], which simply shifts the most likely
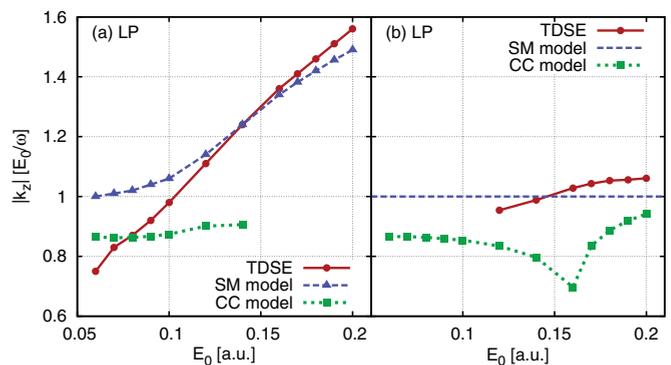

FIG. 4. (Color online) Position of the maximum in the (a) longitudinal distribution $P^{LP}(k_z)$ and (b) lateral width $\sigma^{LP}(k_z)$, plotted versus field amplitude for the LP pulse.
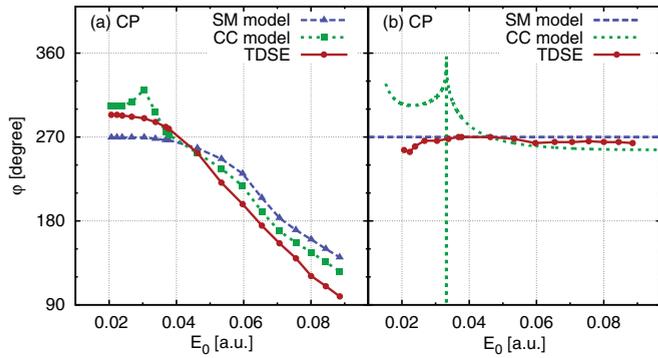
FIG. 5. (Color online) Positions of maxima in the (a) angular distribution $P^{CP}(\varphi)$ and (b) width $\sigma^{CP}(\varphi)$, plotted versus field amplitude for the CP pulse. The vertical line in (b) is due to trajectories that do not escape the core potential.

FIG. 6. (Color online) (a) Maximum widths $\sigma^{LP}_{max}(E_0)$ from the TDSE, from the tunneling product formula, and from the exact adiabatic model versus field amplitude E_0. Also shown is the width at the maximum of the longitudinal distribution. Shown on the right is the width $\sigma^{LP}(k_z)$ versus longitudinal momentum for (b) 1600 nm and $E_0 = 0.10$ a.u., (c) 800 nm and $E_0 = 0.12$ a.u., and (d) 400 nm and $E_0 = 0.14$ a.u. The total ionization probability was approximately 0.5 in each case.

starting time t_0 to earlier times. However, if we compare the TDSE curves to the predictions of the SM model including depletion, we observe that a difference remains. This could indicate some unknown fundamental effects, such as an initial velocity [36]. The shift at small fields is explained mainly by Coulomb corrections. The CC model improves the SM model, except near the barrier-suppression field. For the LP pulse, this could be confirmed only for amplitudes below the barrier-suppression field (due to nonunique mapping from k_z to t_0 for higher fields), which is at approximately 0.157 a.u. in the H atom (the LP calculation) compared to 0.033 a.u. for the soft-core potential (the CP calculation). Note that the large difference between these two values stems mainly from the decoupling in parabolic coordinates for the LP pulse [35]. In contrast to the maxima in the signal, the positions of the maxima in the lateral width depend only weakly on the field amplitude [see Figs. 4 and 5(b)]. They stay close to the position that corresponds to ionization at the peak of the laser field, i.e., $k_z = -E_0/\omega$ and $\varphi = 270°$, respectively. These results demonstrate the robustness of the width against depletion.

Figure 6(a) shows the maximum values of the lateral width $\sigma^{LP}_{max}(E_0)$ versus field amplitude E_0. In agreement with the analysis of the experimental data in Ref. [20], we observe that the widths predicted by the tunneling product formula are consistently too small (also for the few-cycle CP pulse, which is not shown). In contrast, the exact adiabatic model agrees with great accuracy with the TDSE results. To investigate the question of nonadiabaticity, we performed additional
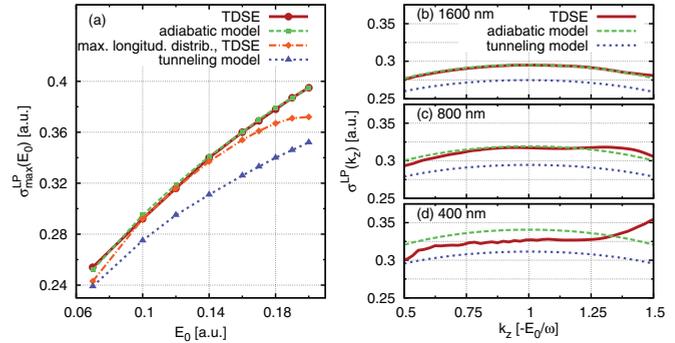
calculations at wavelengths of 400 and 1600 nm [see Figs. 6(b)–6(d)]. For small wavelengths ($\lambda = 400$ nm), we observe deviations of the TDSE widths from the exact adiabatic model. Interestingly, the TDSE tends to predict smaller widths than the adiabatic model, which is in conflict with the trend predicted by nonadiabatic corrections to the tunneling formula [20,25]. In fact, our finding is similar to the small measured nonadiabatic shift [20], which was within the experimental error bars. We mention that we have performed preliminary calculations of the width using the strong-field approximation beyond the saddle-point approximation, showing agreement with the TDSE and not with the tunneling product formula [Eq. (9)].

We have reported a thorough analysis of the lateral width in recollision-free strong-field ionization, leading to the conclusions that (i) the width follows the instantaneous electric field, (ii) it is nearly perfectly adiabatic, and (iii) it is robust against depletion and Coulomb effects. Measurement of the lateral distribution provides a valuable tool to determine field strength and carrier-envelope offset for circularly polarized few-cycle pulses. It will also shine additional light on the search for a tunneling delay time.

[1] D. B. Milošević, G. G. Paulus, D. Bauer, and W. Becker, J. Phys. B **39**, R203 (2006).

[2] F. Krausz and M. Y. Ivanov, Rev. Mod. Phys. **81**, 163 (2009).

[3] E. Goulielmakis, M. Schultze, M. Hofstetter, V. S. Yakovlev, J. Gagnon, M. Uiberacker, A. L. Aquila, E. M. Gullikson, D. T. Attwood, R. Kienberger, F. Krausz, and U. Kleineberg, Science **320**, 1614 (2008).

[4] J. H. Posthumus, Rep. Prog. Phys. **67**, 623 (2004).

[5] G. Sansone, F. Kelkensberg, J. F. Pérez-Torres, F. Morales, M. F. Kling, W. Siu, O. Ghafur, P. Johnsson, M. Swoboda, E. Benedetti, F. Ferrari, F. Lépine, J. L. Sanz-Vicario, S. Zherebtsov, I. Znakovskaya, A. L'Huillier, M. Yu. Ivanov, M. Nisoli, F. Martín and M. J. J. Vrakking, Nature (London) **465**, 763 (2010).

[6] P. B. Corkum, N. H. Burnett, and F. Brunel, Phys. Rev. Lett. **62**, 1259 (1989).

[7] T. F. Gallagher, Phys. Rev. Lett. **61**, 2304 (1988).

[8] G. G. Paulus, W. Becker, W. Nicklich, and H. Walther, J. Phys. B **27**, L703 (1994).

[9] T. Brabec, M. Y. Ivanov, and P. B. Corkum, Phys. Rev. A **54**, R2551 (1996).

[10] S. Popruzhenko and D. Bauer, J. Mod. Opt. **55**, 2573 (2008).

[11] M. Smolarski, P. Eckle, U. Keller, and R. Dörner, Opt. Express **18**, 17640 (2010).

[12] P. B. Corkum, Phys. Rev. Lett. **71**, 1994 (1993).

[13] P. Eckle, M. Smolarski, P. Schlup, J. Biegert, A. Staudte, M. Schoffler, H. G. Muller, R. Dorner, and U. Keller, Nature Phys. **4**, 565 (2008).

[14] C. P. J. Martiny, M. Abu-samha, and L. B. Madsen, J. Phys. B **42**, 161001 (2009).

[15] M. Abu-samha and L. B. Madsen, Phys. Rev. A **84**, 023411 (2011).

[16] P. Dietrich, F. Krausz, and P. B. Corkum, Opt. Lett. **25**, 16 (2000).

[17] P. Eckle, A. N. Pfeiffer, C. Cirelli, A. Staudte, R. Dörner, H. G. Muller, M. Büttiker, and U. Keller, Science **322**, 1525 (2008).

[18] R. Moshammer, B. Feuerstein, W. Schmitt, A. Dorn, C. D. Schröter, J. Ullrich, H. Rottke, C. Trump, M. Wittmann, G. Korn, K. Hoffmann, and W. Sandner, Phys. Rev. Lett. **84**, 447 (2000).

[19] A. Rudenko, K. Zrost, T. Ergler, A. B. Voitkiv, B. Najjari, V. L. B. de Jesus, B. Feuerstein, C. D. Schröter, R. Moshammer, and J. Ullrich, J. Phys. B **38**, L191 (2005).

[20] L. Arissian, C. Smeenk, F. Turner, C. Trallero, A. V. Sokolov, D. M. Villeneuve, A. Staudte, and P. B. Corkum, Phys. Rev. Lett. **105**, 133002 (2010).

[21] N. B. Delone and V. P. Krainov, J. Opt. Soc. Am. B **8**, 1207 (1991).

[22] M. Spanner, O. Smirnova, P. B. Corkum, and M. Y. Ivanov, J. Phys. B **37**, L243 (2004).

[23] C. Smeenk, J. Z. Salvail, L. Arissian, P. B. Corkum, C. T. Hebeisen, and A. Staudte, Opt. Express **19**, 9336 (2011).

[24] A. S. Alnaser, X. M. Tong, T. Osipov, S. Voss, C. M. Maharjan, B. Shan, Z. Chang, and C. L. Cocke, Phys. Rev. A **70**, 023413 (2004).

[25] D. I. Bondar, Phys. Rev. A **78**, 015405 (2008).

[26] M. D. Feit, J. A. Fleck, and A. Steiger, J. Comput. Phys. **47**, 412 (1982).

[27] J. Henkel, M. Lein, and V. Engel, Phys. Rev. A **83**, 051401(R) (2011).

[28] M. Lein, J. Mod. Opt. **58**, 1188 (2011).

[29] D. Farrelley and W. P. Reinhardt, J. Phys. B **16**, 2103 (1983).

[30] V. V. Kolosov, J. Phys. B **20**, 2359 (1987).

[31] J. Rao, W. Liu, and B. Li, Phys. Rev. A **50**, 1916 (1994).

[32] L. D. Landau and E. M. Lifshitz, *Quantum Mechanics* (Butterworth-Heinemann, Oxford, 1977), p. 181.

[33] M. Lewenstein, P. Balcou, M. Y. Ivanov, A. L'Huillier, and P. B. Corkum, Phys. Rev. A **49**, 2117 (1994).

[34] S. Augst, D. Strickland, D. D. Meyerhofer, S. L. Chin, and J. H. Eberly, Phys. Rev. Lett. **63**, 2212 (1989).

[35] R. Shakeshaft, R. M. Potvliege, M. Dörr, and W. E. Cooke, Phys. Rev. A **42**, 1656 (1990).

[36] M. Odenweller, N. Takemoto, A. Vredenborg, K. Cole, K. Pahl, J. Titze, L. P. H. Schmidt, T. Jahnke, R. Dörner, and A. Becker, Phys. Rev. Lett. **107**, 143004 (2011).